# Observation of High Soft X-Ray Drive in Large-Scale Hohlraums at the National Ignition Facility

J. L. Kline,[1] S. H. Glenzer,[2] R. E. Olson,[3] L. J. Suter,[2] K. Widmann,[2] D. A. Callahan,[2] S. N. Dixit,[2] C. A. Thomas,[2] D. E. Hinkel,[2] E. A. Williams,[2] A. S. Moore,[4] J. Celeste,[2] E. Dewald,[2] W. W. Hsing,[2] A. Warrick,[2] J. Atherton,[2] S. Azevedo,[2] R. Beeler,[2] R. Berger,[2] A. Conder,[2] L. Divol,[2] C. A. Haynam,[2] D. H. Kalantar,[2] R. Kauffman,[2] G. A. Kyrala,[1] J. Kilkenny,[5] J. Liebman,[2] S. Le Pape,[2] D. Larson,[2] N. B. Meezan,[2] P. Michel,[2] J. Moody,[2] M. D. Rosen,[2] M. B. Schneider,[2] B. Van Wonterghem,[2] R. J. Wallace,[2] B. K. Young,[2] O. L. Landen,[2] and B. J. MacGowan[2]

[1]*Los Alamos National Laboratory, Los Alamos, New Mexico 87545, USA*
[2]*Lawrence Livermore National Laboratory, Livermore, California 94550, USA*
[3]*Sandia National Laboratory, Albuquerque, New Mexico 87185, USA*
[4]*Atomic Weapons Establishment, Aldermaston, RG74PR, United Kingdom*
[5]*General Atomics, San Diego, California 92121, USA*

(Received 30 April 2010; published 25 February 2011)

The first soft x-ray radiation flux measurements from hohlraums using both a 96 and a 192 beam configuration at the National Ignition Facility have shown high x-ray conversion efficiencies of ~85%–90%. These experiments employed gold vacuum hohlraums, 6.4 mm long and 3.55 mm in diameter, heated with laser energies between 150–635 kJ. The hohlraums reached radiation temperatures of up to 340 eV. These hohlraums for the first time reached coronal plasma conditions sufficient for two-electron processes and coronal heat conduction to be important for determining the radiation drive.

DOI: 10.1103/PhysRevLett.106.085003 PACS numbers: 52.50.Jm, 52.38.Ph, 52.70.La

High-energy density laser experiments use hohlraums made of high-$Z$ materials to convert laser energy into soft x rays with an approximately Planckian radiation spectrum. The hohlraum x-ray radiation is used to drive a wide range of physics experiments to study equations of state or material dynamics [1], hydrodynamic instabilities [2,3], radiation transport [4,5], and astrophysical processes [6]. The advantage of converting the laser to x rays lies in the fact that hohlraum x-ray sources provide a uniform illumination for physics experiments, eliminating laser imprint due to spatial variations in the intensity of the impinging laser light. The penalties in converting the optical laser light to x-ray radiation include losses in heating the hohlraum wall and incomplete conversion of the laser light to x rays. The completion of the National Ignition Facility (NIF) [7] opens new possibilities to scale experiments to larger sizes and to higher radiation fluxes [8] allowing exploration of new physics regimes.

The conversion of laser light to x rays in a hohlraum is described by the following power balance equation:

$$P_{\mathrm{rad}} = \eta(P_l - P_{\mathrm{backscatter}}) = \sigma T_{\mathrm{rad}}{}^4(A_w(1-\alpha) + A_h), \quad (1)$$

where $P_{\mathrm{rad}}$ is the total x-ray production, $\eta$ is the x-ray conversion efficiency of the laser power to soft x rays, $P_l$ is the laser power, $P_{\mathrm{backscatter}}$ is the backscattered laser power not coupled to the hohlraum, $\sigma$ is Boltzmann's constant, $T_{\mathrm{rad}}$ is an effective temperature characterizing the total x-ray flux, $A_w$ is the area of the hohlraum wall, $A_h$ is the area of the laser entrance holes, and $\alpha$ is the wall albedo defined as the ratio of the emitted x-ray flux from the hohlraum wall to that incident on the wall. Simply, the left-hand side of Eq. (1) represents the source of x-ray power which is converted from the incident laser power and the right hand side represents losses of x-ray power due to absorption by the hohlraum wall through the driven heat wave or Marshak wave and to x rays escaping through the laser entrance holes. For experiments, the incident laser power, the radiated power escaping through the laser entrance holes, and the backscattered laser power are measured, leaving the conversion efficiency and wall albedo to be inferred using the above equation. The conversion efficiency describes the fraction of absorbed laser power that is converted into soft x-ray flux. Absorbed laser power not converted into x rays is retained in the hot, under-dense coronal plasma such that $P_{\mathrm{rad}} = P_l - P_{\mathrm{backscatter}} - P_{\mathrm{corona}}$ where $P_{\mathrm{corona}} = (1-\eta)(P_l - P_{\mathrm{backscatter}})$. It should also be noted that the addition of an experimental physics package or a capsule in the hohlraum contributes an additional loss term reducing the radiation temperature.

As hohlraums increase in size with the available energy on the NIF, the volume of the coronal plasma increases more rapidly than the wall area and the temperature of the plasma filling the hohlraum rises because of longer inverse bremsstrahlung scale length. NIF scale hohlraums have ~8 times (or more) the wall area and ~20 times the volume of the Nova or Omega scale hohlraums. Consequently, for hohlraums filled with plasma our simulations indicate the fraction of total energy stored in the corona is significantly greater on NIF than on Nova or Omega; ~15%–30% on NIF versus 5%–10% on Nova. Because of this, predictions of NIF hohlraum radiation temperatures are more sensitive

 

to models that change the coronal energy than previous Nova or Omega hohlraums [9]. Two important processes affecting $P_{\mathrm{corona}}$ are plasma emissivity and electron heat conduction. There are several physics models for both of these in the radiation hydrodynamics codes used to simulate hohlraum targets. Discrepancies in the simulations with different models of emissivity and electron heat conduction which could not be differentiated by smaller hohlraums now become apparent as demonstrated by comparisons of the simulations with the data from the experiments presented here.

In this Letter, we report on the first high-energy density large-scale vacuum hohlraum experiments showing x-ray radiation fluxes 20%–30% higher than anticipated using conservative models benchmarked by smaller hohlraum targets on Nova and Omega [10–13]. We find that simulations using less conservative atomic physics and electron heat transport models agree with the measurements and indicate a hohlraum x-ray conversion efficiency of ~85%–90%.

In this study, the hohlraums were heated with NIF's 192 laser beams of 351 nm laser light. The beams are arranged into four beam cones for both the lower and upper hemispheres of the spherical target chamber. The two inner beam cones are at 23.5° and 30° with respect to the vertical axis while the outer beam cones are at 44.5° and 50° (Fig. 1). There are twice as many beams in the outer beam cones as in the inner cones so that approximately two thirds of the total available laser energy is contained in the outer beams. The total laser energy and power delivered by each quad is measured with ±2% and ±3% accuracy, respectively. The experiments were performed with both a 96- and a 192-beam configuration with energies ranging from 150–635 kJ at 351 nm in 2 ns square pulses. For the 96-beam configuration, only the beams at 30° and 50° were used. The beams were smoothed using polarization smoothing, 45 GHz smoothing by spectral dispersion (SSD), and continuum phase plates (CPPs) [14,15]. The CPPs in each cone produced a different elliptical spot size at best focus giving intensity ranges of ~1.8–4.0 × $10^{14}$ W/cm$^2$ for the 23.5° beams, ~2.0–4.5× $10^{14}$ W/cm$^2$ for the 30° beams, ~4.3–9.4 × $10^{14}$ W/cm$^2$ for the 44.5° beams, and ~4.9–10.8 × $10^{14}$ W/cm$^2$ for the 50° beams. Backscatter diagnostics were fielded on the high-energy shots for a single quad of beams in both the 30° and 50° beam cones. We find that the total reflected energy due to laser backscatter instabilities is less than 2% of the total incident energy. In addition, a static x-ray imager consisting of a four pinhole x-ray camera, was employed to measure the focal spot locations of the beams irradiating the inside of the hohlraum [16].

The gold vacuum hohlraum targets have a wall thickness of 25 microns, a length of 6.4 mm, an inner diameter of 3.55 mm and a laser entrance hole diameter of 2.65 mm (Fig. 1). The hohlraums were aligned along the vertical axis of the target chamber. The soft x-ray radiation drive was measured using the Dante diagnostic [17]. Dante is

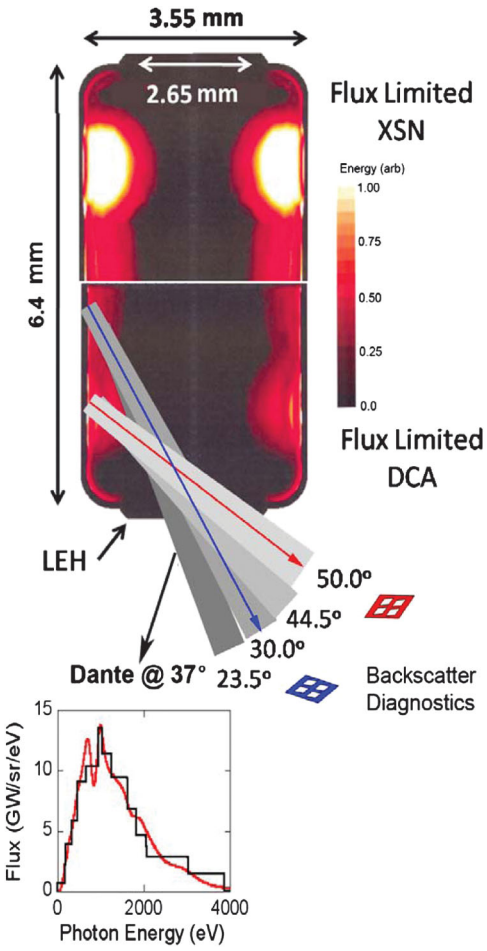


FIG. 1 (color). Plot shows the experimental configuration of the targets including the four beam cones and dimensions of the large hohlraums. Included in the figure is a calculation of the specific energy stored in the coronal plasma for the flux-limited XSN (top) model with a flux limit of 0.05 and DCA (bottom) models with a flux limit of 0.15 at 2 ns in the laser pulse for 635 kJ. The spectrum at peak x-ray flux with a radiation temperature of 340 eV and a x-ray power of 19 600 GW/sr is included as measured by (red solid line) Dante and overlaid with the (black solid line) calculated spectrum using the DCA model and a flux limit of 0.15.

an 18 channel, absolutely calibrated, broadband soft x-ray spectrometer, which uses signals filtered by combinations of x-ray edge filters, mirrors, and diodes to determine the flux in different spectral regions [18]. A spectral unfold algorithm uses the measured fluxes in each channel to reconstruct the spectrum of the radiation exiting the hohlraum laser entrance hole. An example of the spectral reconstruction is included in Fig. 1. We use the integrated flux up to 13 keV as a measure of the total flux.

Figure 1 also shows the calculated specific energy in the coronal plasma for two radiation-hydrodynamic simulations using different models in a two dimensional $r$-$z$ geometry for the hohlraums. The calculations of the specific energy in the coronal plasma on the top half of the image uses the conservative radiation-hydrodynamic modeling that agreed well with Nova or Omega data.

It employs the nonlocal thermodynamic equilibrium (NLTE) XSN average-atom atomic physics model [19] and an electron heat transport flux limiter of 0.05. The XSN average-atom atomic physics model tracks the shell populations of the principle quantum levels averaged over all ionic states and in its default mode does not include two-electron processes, i.e., dielectronic recombination. Shown on the bottom half of the image is a calculation that uses a NLTE detailed configuration accounting (DCA) atomic physics model accounting for two-electron processes with a flux-limiter of 0.15. Unlike the XSN model, the DCA model solves rate equations for populations of the most dominant excited states for all ionization states. Recent improvements to the DCA model [20] have increased computing efficiency so that it can be routinely used in integrated simulations. Both calculations use a flux-limited heat diffusion model that chooses on a per zone basis in the simulation the minimum of either the Spitzer-Härm electron heat flux, $k_{\mathrm{SH}}\nabla T_e$ where $k_{\mathrm{SH}}$ is the Spitzer-Härm conductivity and $T_e$ is the electron temperature or a fraction of the free streaming heat flux, $f v_e n_e T_e$, where $f$ is the flux-limiter value, $v_e$ is the electron thermal velocity, and $n_e$ is the electron density. The value of the flux limiter affects the flow of energy carried by the electrons. It is clear that the specific energy in the coronal plasma is higher in flux-limited XSN than with the DCA model.

The time history of the measured x-ray radiation flux for a hohlraum with 635 kJ of energy is shown Fig. 2 The measured flux is compared with simulations that use flux-limited XSN and DCA models with flux limits of 0.05, 0.15, and 1.0 where the flux limit of 1.0 is the free streaming limit. Applying a DCA versus a XSN model with the prior standard flux limit of 0.05 only accounts for about 1/2 of the increase in the measured flux. The DCA model with a flux limit of 0.15 is in best agreement with the experimental results at the peak of the laser pulse. At the same time, there is little difference between the flux limit values of 0.15 and 1.0 indicating that heat transport in the coronal plasma is essentially Spitzer-like and not free streaming. The peak fluxes for both of these simulations, as well as the measurements, on average are ~20%–30% larger than the peak radiation fluxes predicted by the XSN models regardless of the flux limit. This illustrates that both changes in the atomic physics model and heat conduction are necessary to bring the simulations in agreement with the peak x-ray flux measurements. Additional comparisons with simulations including variations of atomic physics model parameters and changes in the flux limiter showed that neither changes in the flux limiter nor the atomic physics modeling alone could match the levels of peak radiation flux observed in the experiments. Applying the flux-limited DCA model with a flux limit of 0.15 to all of these large-scale hohlraum experiments shows good agreement with the experimental measurements (Fig. 3).

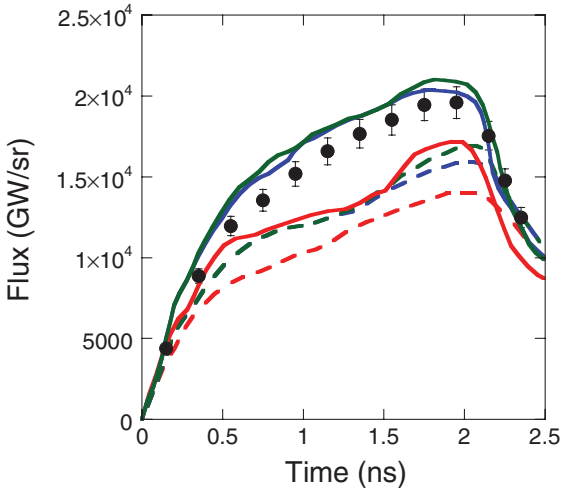


FIG. 2 (color). (●) Experimental measurements compared with radiation-hydrodynamic simulations of vacuum hohlraums on the NIF with the XSN atomic physics model with a flux limiter of (red dashed line) 0.05, (blue dashed line) 0.15, and (green dashed line) 1.0 along with calculations using a DCA model with a flux-limiter of (red solid line) 0.05, (blue solid line) 0.15, and (green solid line) 1.0.

The agreement between the measurements and the simulations using the flux-limited DCA atomic physics model with the flux limit of 0.15 is an indication that higher coronal plasma emissivities lead to cooler plasmas absorbing less specific energy and allowing more x rays to heat the wall. Higher hohlraum wall temperatures lead to an increase in the measured x ray flux. The change in the flux-limiter value has a similar effect with respect to electron heat transport. Increasing the flux limit allows more of the laser energy absorbed by the corona to flow to the wall through electron heat conduction. Both changes lead to an increase in the x-ray conversion efficiency as a result of a factor of 2 less specific energy being absorbed by the coronal plasma. This is shown by the comparison of the DCA atomic physics model with a flux limit of 0.15 and the

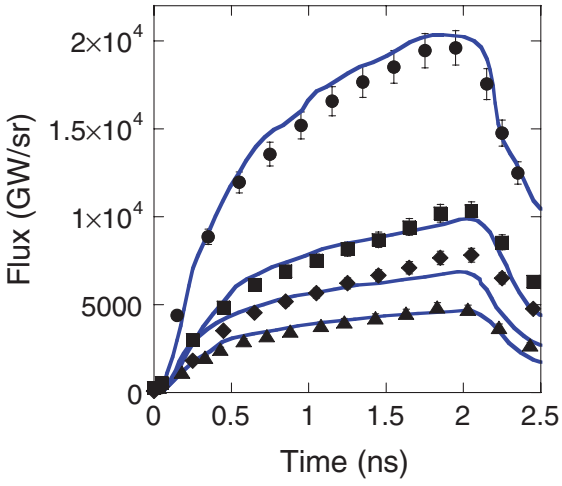


FIG. 3 (color). Comparison of the time histories of the measured flux with (blue solid line) simulations using the DCA model with a flux limiter of 0.15 for increasing laser energies of (▲) 150, (◆) 233, (■) 308, and (●) 635 kJs.

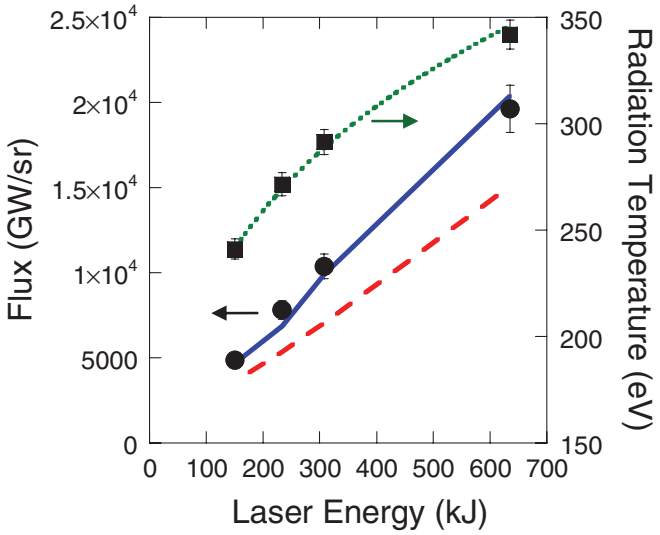


FIG. 4 (color). Scaling of the (●) measured peak radiation fluxes compared with that of flux-limited XSN simulation with a flux limit of (red dashed line) 0.05 and of the DCA model with a flux limit of (blue solid line) 0.15. The peak radiation temperatures (■) measured with (green dashed line) a curve fit using Eq. (1) at 2 ns with the wall albedo of 90% inferred from simulation that gives a conversion efficiency of ~88%.

XSN atomic physics model with a flux limit of 0.05 in Fig. 1.

Past experimental measurements of the plasma conditions in laser produced high-$Z$ foil plasmas using Thomson scattering have also shown the discrepancy between the DCA and XSN models. In those experiments, the DCA model was a better fit to the measurements [21,22]. Those experimental measurements also show the deficiency with the flux-limited diffusion model. Since the flux-limiter is typically fixed during the entire simulation, the model cannot account for changing plasma conditions in the hohlraum that would affect the heat conduction, while a nonlocal heat conduction model may provide better agreement over the duration of the experiment [23,24]. Other recent experiments to measure the x-ray conversion efficiency using spherical gold targets have also required an increase in the flux limit from 0.05 to 0.15 in order to get agreement between the simulations and the experimental measurements [25].

The experimental results presented here show that vacuum hohlraums continue to "work" at energy levels some 10–20 times greater than previously used (while keeping the energy density approximately fixed). The laser energy scaling of the peak radiation fluxes and temperatures is summarized in Fig. 4. They also show the increased importance, as we increase scale size, of the energy stored in the corona that fills the hohlraum and the need to more accurately model NLTE emissivity and electron heat transport. We have also demonstrated a peak radiation temperature on NIF of 340 eV, that could only be achieved previously with very small hohlraums [26]. An estimate of the conversion efficiency, ~88%, can be inferred by fitting the power balance Eq. (1) to the peak radiation temperatures, using the laser power at the peak of the pulse and a wall albedo of 90%. The conversion efficiency of the individual points ranges from ~85%–90%. Such values have been previously estimated from hohlraum simulations by Suter *et al.* [13]. For this estimate of the conversion efficiency, it should be noted that the albedo was deduced from the simulations.

The high radiation temperatures reported here and the increase in hohlraum size enable significantly larger scale x-ray driven physics applications. This, in turn, enables a wider variety of physics applications that can take advantage of larger scale sizes to discern physical features and higher ablation pressures to reach new regimes. For example, at the radiation temperatures reported here, this leads to pressures on the order of twice that of Nova or Omega hohlraums which had 5x smaller linear dimensions for experimental physics packages.

We wish to thank the NIF operations/laser team for their support. This work was performed under the auspices of the U.S. DOE by LANL under contract DE-AC52-06NA25396, by LLNL under contract DE-AC5 2-07NA27344, and by SNL under contract DE-AC04-94AL85000.

[1] B. Remington *et al.*, Metall. Mater. Trans. A **35**, 2587 (2004).
[2] D. K. Bradley *et al.*, Phys. Plasmas **16**, 042703 (2009).
[3] J. A. Cobble, Phys. Plasmas **13**, 056304 (2006).
[4] C. A. Back *et al.*, Phys. Rev. Lett. **84**, 274 (2000).
[5] P. Keiter *et al.*, Phys. Plasmas **15**, 056901 (2008).
[6] P. Rosen *et al.*, Astrophys. Space Sci. **322**, 101 (2008).
[7] E. Moses and C. R. Wuest, Fusion Sci. Technol. **47**, 314 (2005).
[8] E. L. Dewald *et al.*, Phys. Rev. Lett. **95**, 215004 (2005).
[9] L. Suter *et al.*, in *Atomic Processes in Plasmas: Proceedings of the 16th International Conference on Atomic Processes in Plasmas* (AIP, Monterey, California, 2009).
[10] E. Dattolo *et al.*, Phys. Plasmas **8**, 260 (2001).
[11] C. Decker *et al.*, Phys. Rev. Lett. **79**, 1491 (1997).
[12] L. J. Suter *et al.*, Phys. Rev. Lett. **73**, 2328 (1994).
[13] L. J. Suter *et al.*, Phys. Plasmas **3**, 2057 (1996).
[14] C. A. Haynam *et al.*, Appl. Opt. **46**, 3276 (2007).
[15] J. A. Menapace *et al.*, in *Laser-Induced Damage in Optical Materials: 2003* (SPIE, Boulder, CO, USA, 2004).
[16] M. D. Landon *et al.*, Rev. Sci. Instrum. **72**, 698 (2001).
[17] E. L. Dewald *et al.*, Rev. Sci. Instrum. **75**, 3759 (2004).
[18] K. M. Campbell *et al.*, Rev. Sci. Instrum. **75**, 3768 (2004).
[19] W. A. Lokke and W. H. Grasberger, Report No. LLNL UCRL-52276, 1977.
[20] H. A. Scott and S. B. Hansen, High Energy Density Phys. **6**, 39 (2010).
[21] S. H. Glenzer *et al.*, Phys. Rev. Lett. **82**, 97 (1999).
[22] S. H. Glenzer *et al.*, J. Quant. Spectrosc. Radiat. Transfer **65**, 253 (2000).
[23] G. Schurtz *et al.*, Phys. Rev. Lett. **98**, 095002 (2007).
[24] G. P. Schurtz, P. D. Nicolai, and M. Busquet, Phys. Plasmas **7**, 4238 (2000).
[25] E. L. Dewald *et al.*, Phys. Plasmas **15**, 072706 (2008).
[26] D. E. Hinkel *et al.*, Phys. Rev. Lett. **96**, 195001 (2006).